Coupled Rheology, Filament Contact, and Sintered Response in Direct-Written Hard-PZT Ceramics

Dr. Rafay Tallat[1,*] and Dr. Pooja Sharma[1]

[1] Indian Institute of Technology Delhi Hauz Khas,New Delhi-110016
* Correspondence: rafya.tal@iitd.ac.in

Abstract: Hard lead zirconate titanate (PZT) ceramics need more than just continuous extrusion in order for direct ink writing (DIW) to be successful. The printed ring needs to be capable of maintaining filament line shape after shear, restricting inter-strut pathways for liquid-phase transport, avoiding the formation of endpoint defects, densifying without degrading phase formation, and developing piezoelectricity during subsequent poling. This work investigates a range of hard-PZT inks having six different compositions, comprising a base ratio of 50, 52.5, and 55 vol% solids at either 1 or 2 wt% dispersant concentration, to determine whether or not there exists a formulation combination and DIW machine setting that would allow the fabrication of a printed part of high density and similar piezoelectric behavior to die-pressed parts. The full dataset includes formulation ratios, Herschel–Bulkley model parameters, oscillatory yield stress, maximal storage modulus value, extrusion pressure, travel speed, nozzle diameter, line-shape observation, endpoint defect formation, relative density, phase/microstructure observation, and d_{33}. As a full process chain is considered, from suspension preparation to printed ceramic functionality, each ink composition will be evaluated on the basis of the specific problem it causes. The formulations of P50D2 and P52.5D2 are too soft, while P55D1 is too stiff and overly sensitive to pressure. P55D2, on the other hand, represents a compromise between the aforementioned formulations, with high dispersant partitioning and poor printability behavior. Only P52.5D1 is located inside the process window, consisting of 52.5 vol% solids and 1 wt% dispersant, with an oscillatory yield stress of 154.23 Pa, achieving $G'_{\max} = 146\,680$ Pa, giving a height for printable ink of approximately 3.42 mm, printing through a 420 µm nozzle at 5 mm s^{-1} and roughly 0.045 MPa extrusion pressure. Sintered at 1200 °C, P52.5D1 prints yield a dense ring with relative density of 97.59(46) %, approximately 0.14 percentage points below the die-pressed sample, retaining $d_{33} \approx 268(10)$ pC/N. The main conclusion drawn here is that functional dense hard-PZT DIW can be achieved through a combination of material-motion-sintering window; the ink should recover elastic deformation, the printed line should interact with adjacent filament, and the sintered body should sustain density and piezoelectricity.

Keywords: direct ink writing, hard-PZT ceramics, rheology, filament geometry, sintered density, piezoelectric response

Citation: Dr. Rafay Tallat and Dr. Pooja Sharma. 2023. Coupled Rheology, Filament Contact, and Sintered Response in Direct-Written Hard-PZT Ceramics. *TK Techforum Journal (ThyssenKrupp Techforum)* 2023(2): 1–12.

Received: January-24-2023
Accepted: April-02-2023
Published: September-30-2023

1. Introduction

Whereas the shaping potential of ceramic additive manufacturing lies in achieving geometries unattainable by pressing, casting, slip forming, or machining due to complex internal channels, curvature of the walls, distribution of mass, or custom device ring structure, the manufacture of functionally graded ceramics raises additional challenges. In this context, the green state should remain stable throughout the drying process, be able to eliminate organic components without damage, densify through sintering, and maintain the phase and structure that provide the desired performance [1–5]. Therefore, dense ceramic additive manufacturing needs to be analyzed as a whole production chain, beginning with the preparation of the paste and ending with material performance.

Direct ink writing (DIW), otherwise called robocasting or extrusion-based ceramic writing, makes it especially evident. The paste used should have sufficient flow properties

inside the nozzle, exhibit continuous flow, recover its elasticity almost immediately after deposition, and provide mechanical stability to adjacent filaments or subsequent layers of ink. Fundamental research into direct colloidal writing confirmed that ceramic parts could be produced by managing the interplay between particle interactions and deposition process parameters [6–9]. Further research into dense ceramic pastes found an important balance in that a poorly structured paste might be easy to print but deform while a highly structured one might be easy to deposit but require excessive pressure [10–13].

The challenge becomes even greater in lead zirconate titanate (PZT), where the performance of the printed component is related to electromechanical response, not just geometry. PZT continues to be an important material for piezoceramic actuator, sensor, transducer, acoustic, and energy harvester applications due to its ferroelectric switching behavior, high dielectric constant, and excellent electromechanical coupling [14–17]. The useful properties depend on composition, grain growth, relative density, stoichiometry, pore microstructure, and polarization history [18–21]. In other words, it is a success only if the printing process produces a highly dense PZT ceramic with measurable piezoelectric activity.

In recent papers on printing piezoelectric ceramics, advances have been made in paste extrusion processes, DIW architectures, macroporous piezoceramics, and dense functional ceramics [22–27]. They also demonstrate why simply classifying a ceramic powder by its printability/unprintability will not suffice for hard-PZT rings. The paste might have uniform distribution but inadequate cohesive strength, sufficient stiffness for maintaining the geometry but not sufficiently fluid to handle, homogenous structure but internal weakness to channel formation, fully dense sintering yet susceptibility to phase instability or depolarization. Thus, the research question under consideration can be specified: *which composition and processing conditions in the six-ink hard-PZT matrix combination will produce the suspension cohesion, recoverable rheology, filament contact control, endpoint defect suppression, high density, and d_{33} properties equivalent to those of die pressing?*

Increasing the loading of ceramics results in the less liquid and organic content removed before sintering, but it increases the low-shear resistance and pressure requirements. More dispersant helps with the separation of particles, yet too much could compromise the structure of the particle network, needed to sustain the shape after shearing [28,29]. Then it comes down to how nozzle diameter, travel speed, and pressure make the ink behave like a well-defined filament, or otherwise over-filled or starved. Last, the firing should densify the ring in a lead-rich environment without inducing phase instabilities and weak layers [30–32].

This work investigates six aqueous hard-PZT inks based on the ratios of 50, 52.5, or 55 vol% solids, and 1 or 2 wt% of dispersant. The comparison between formulations involves Herschel–Bulkley flow parameters, oscillatory yield stress, storage modulus, pressure, travel speed, filament ratio, defect behavior of the end point, relative density of the sintered ring, microstructural analysis, phase stability, and d_{33} performance. In other words, we seek to find the physical compatibility at each stage of processing rather than suggest a universally good ink formula regardless of the choice of the powder, binder, nozzles, and thermal regime.

The schematic representation of the process, Figure 1, describes the specimen-centered approach applied throughout the present research. Here, six hard-PZT inks are fed into the printing process resulting in one annular sample that is subsequently fired to give a ring-shaped ceramic. The image is deliberately simple, giving the reader a visual understanding of the material-to-ceramic flow before any numerical screening occurs.

The photographical steps in Figure 1 can help us to understand that the ring is the key object investigated in this work since homogeneous ink feeding will result in a continuous circular filament, the green ring should be kept intact during both drying and burnout, and the fired ring should be dense enough for poling. Thus, the following figures are related to the same specimen going through the steps from ink printing to ceramic body functionality.

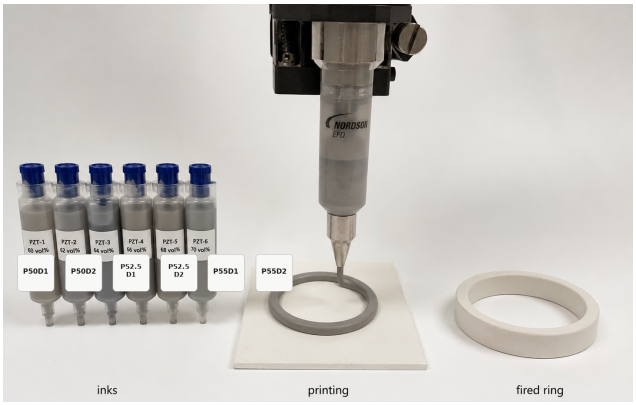

Figure 1. Ink printing route.

2. Ink Composition and Processing Parameters

For the production of hard-PZT inks, it was necessary to use the PZT powder, 5 wt% aqueous binder, glycerol, and dispersant DISPERBYK-180 [33]. The mean particle size of the powder was 0.60 µm. The composition matrix includes three PZT solid fractions (50, 52.5, 55 vol%) and two amounts of the dispersant (1 and 2 wt%). By pneumatic robot-assisted deposition, ring specimens with an outer diameter around 12.5 mm and an inner diameter around 6.5 mm were printed. Next, the printed specimens were dried and burn-out at 600 °C. The sintering was conducted under lead-rich atmosphere from 1100 °C up to 1300 °C. In addition, the conventionally processed specimens were die-pressed, and cold isostatic pressing was studied for the printing process [33].

This analysis follows a structured format according to four process evaluations. The first evaluation considers composition and partition of liquids, since binder, glycerol, and dispersant define the equilibrium between particle separation and cohesion after extrusion. The second evaluation considers rheological properties through Herschel–Bulkley yield stress, flow index, consistency, oscillatory yield stress, and maximum storage modulus. The third evaluation considers the extrusion and deposition processes using nozzle diameter, travel velocity, pressure, line-width ratio, line-height ratio, and end-point evaluation. Finally, the fourth evaluation concerns the viability of the printed ring following burnout, sintering, phase retention, consolidation, and d_{33} evaluation. This process prevents the acceptance of an ink simply due to the presence of a certain desirable property.

The composition values for each of the six inks are given in Table 1. Although the dispersant-to-liquids ratio has been kept as well, since it defines the difference between similar formulations according to their solids loading. A larger value may be beneficial for achieving easy flow initiation, but also results in a reduction of the elastic network of particles which should recover as soon as the printing is over.

Table 1. Six PZT ink compositions.

Ink	**PZT** (vol%)	**Disp.** (wt%)	**PVA sol.** (vol%)	**Disp./other** ratio	**Other liquids** (vol%)	**Glycerol** (vol%)
P50D1	50.0	1	3.61	0.0778	41.39	5.00
P50D2	50.0	2	7.22	0.1690	37.78	5.00
P52.5D1	52.5	1	3.79	0.0870	38.96	4.75
P52.5D2	52.5	2	7.58	0.1900	35.16	4.75
P55D1	55.0	1	3.97	0.0970	36.53	4.50
P55D2	55.0	2	7.94	0.2140	32.55	4.50

The values provided in Table 1 indicate that increasing the dispersant amount affects the liquid structure of the paste rather than its additive content alone. For instance, the ratio between the dispersant and other liquids increases from 0.0778 to 0.1690 when using 50 vol% PZT and from 0.0970 to 0.2140 when using 55 vol%. Consequently, the 2 wt% ink

formulations are not only less viscous but have a different deflocculation-to-recovery ratio, which is especially significant when building up stiffness after deposition.

Table 2 provides a description of the six inks' rheological characteristics. The Herschel–Bulkley constants represent the paste's resistance to shear flow, whereas the oscillatory yield stress and G'_{max} reflect the elastic structure recovered by the paste after extrusion through a nozzle. These two parameters are essential since a highly concentrated ceramic paste is capable of flowing in shear and deforming unless it regains its stiffness after deposition [29,34–36].

Table 2. Rheological descriptors of the six inks.

Ink	σ_y **(HB)** (Pa)	n	k (Pa s^n)	σ_y **from** G' (Pa)	G'_{max} (Pa)
P50D1	79.72	0.39	95.09	104.84	56512
P50D2	28.12	0.65	39.43	23.18	6352
P52.5D1	112.67	0.54	150.32	154.23	146680
P52.5D2	35.98	0.55	96.36	49.05	8877
P55D1	267.84	0.49	307.82	229.22	253260
P55D2	68.66	0.54	153.13	97.98	10899

The characteristics reported in Table 2 determine the key problem faced by dense PZT printing. Both P50D2 and P52.5D2 feature a low oscillatory yield stress and a low maximum value of elastic modulus G'_{max}. These two parameters increase susceptibility to any kind of deformations after extrusion. On the other hand, P55D1 features a high value of both of them, favoring self-support but increasing pressure sensitivity and clogging probability. The useful middle position in terms of rheological parameters is occupied by P52.5D1. Its strength post-extrusion is greater compared to the soft 2 wt% dispersant ink, but still does not reach the extremes seen with P55D1. Therefore, P52.5D1 becomes the candidate for further considerations, providing numerical justification for the choice.

The connection between physical quantities characterizing materials and effects at a smaller scale is made by flow and geometrical equations. The effective shear rate at the end of the nozzle can be calculated using

$$\dot{\gamma} = \frac{4S}{r}, \tag{1}$$

where S represents the printing speed, whereas r is the nozzle radius. As one can see from Eq. (1), the variation in both these parameters will result in an entirely different shear rate for the same type of ink. An ink formulation recovering sufficiently under certain conditions of printing through a nozzle of a particular size may recover differently if the size changes or the printing speed is increased. This relationship highlights that the motion program plays an important role here.

Minimum pressure to overcome static friction before the onset of flow is estimated as

$$P_{min} = \frac{4L\sigma_y}{D}, \tag{2}$$

where L is nozzle length, D is nozzle inner diameter, and σ_y is yield stress [33,37,38]. Eq. (2) provides the conversion of yield stress to extrusion load. The larger the σ_y, the better the slump resistance. At the same time, a higher value of σ_y increases the pressure that is required for both initiating and sustaining extrusion. Such tradeoff makes it possible to understand why an ultra-strong ink may be inferior to a moderate ink in terms of extrusion printing.

The height of printable ink, h_{max}, can be assessed by

$$h_{max} = \frac{\sigma_y}{\rho g}. \tag{3}$$

Here ρ is the density, and g denotes the gravitational constant [11,33]. This equation does not aim to describe all the printed forms. Rather, Eq. (3) offers a means to order inks based on their resistance to gravitational distortion. Within this research, such an estimate proves meaningful as an indicator of extrusion stability.

Line geometry is defined by two ratios,

$$\Lambda_w = \frac{w}{D}, \qquad \Lambda_h = \frac{h}{D}, \tag{4}$$

in which w stands for the line width, and h denotes the line height. Line geometry is thus turned from an aesthetic property into a process one using Eq. (4). High values of Λ_w indicate an excess of spreading/overprinting, whereas large Λ_h might result in reduced interline contact and creation of channels between filaments. The advantageous configuration, hence, is neither the thinnest nor the tallest line.

The difference in relative density between the direct writing and die pressing process can be expressed as

$$\Delta\rho_{\text{rel}} = \left|\rho_{\text{rel}}^{\text{DIW}} - \rho_{\text{rel}}^{\text{press}}\right|, \tag{5}$$

with $\rho_{\text{rel}}^{\text{DIW}}$ and $\rho_{\text{rel}}^{\text{press}}$ being the relative densities of the printed and die pressed specimens, respectively. With Eq. (5), the comparison can be attributed to manufacturing processes. Small $\Delta\rho_{\text{rel}}$ means the gain of geometric freedom comes from non-consolidated structure, while big $\Delta\rho_{\text{rel}}$ implies the printed ring is still a nice shape but a poor ceramic body.

The above equations define the relation among measured quantities without measuring. In general, the six ink composition, the rheological parameters and the extrusion behaviors, line contact performance and density comparison are tied by these equations together. Therefore, the results are reported as a combined analysis on the manufacturing process.

These two process parameters are illustrated in Figures 2 and 3. The syringe view depicts the six different inks that have been prepared, while the extruded line illustrates the differences between the inks in terms of recovery, straightness, and surface quality using the numbers obtained from rheological measurements.

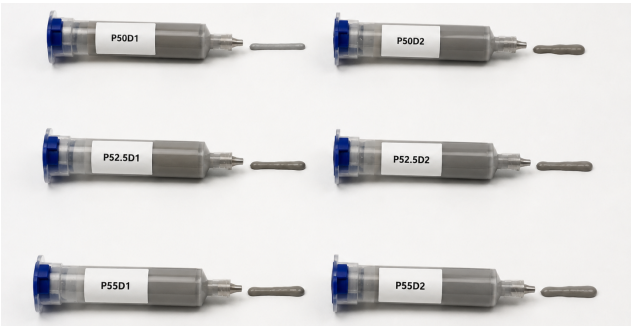

Figure 2. Six prepared hard-PZT inks.

We have illustrated the different inks in terms of their compositions in a visual manner. Since all syringes in the picture above contain similar grey-colored PZT suspensions, a choice among the formulations cannot be made based on their appearance. The labels correspond to the solids and dispersant levels in Table 1, and the important distinction is hidden inside the liquid partitioning: the 2 wt% dispersant inks have a higher dispersant-to-other-liquid ratio, whereas P52.5D1 preserves a more useful balance between particle separation and post-extrusion cohesion.

The extruded-line test in Figure 3 provides the physical interpretation of Table 2. Inks of low structures tend to have a structure that is easy to disrupt, while those of high structures may create uneven surfaces and unfavorable delivery systems. The filament of P52.5D1 can be described as the smoothest in the comparison, as it is supported by the

results that show its oscillatory yield stress being sufficient for recovery without going too stiff as P55D1.

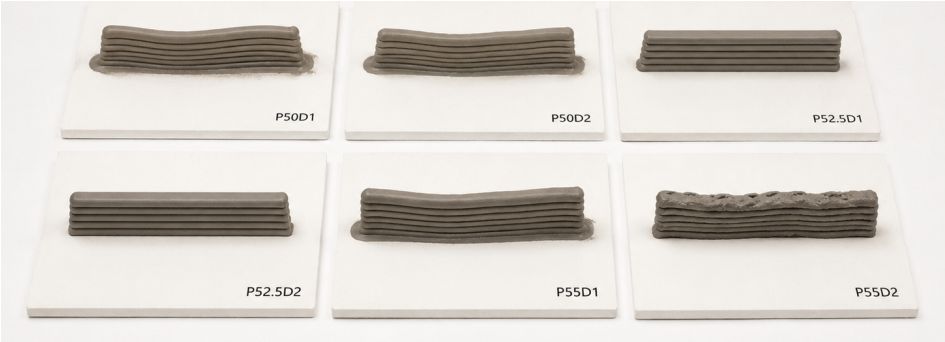

Figure 3. Extruded multilayer filaments.

The retained printing condition is briefly summarized in Table 3. The relation between the ink composition and various physical parameters is provided in order to understand why each of them is important in the next section.

Table 3. Process window and ceramic outcome.

Category	Process status	Manufacturing interpretation
Ink retained after all process checks	P52.5D1, 52.5 vol% solids and 1 wt% dispersant	Balanced recovery, flow resistance, and solids content
Secondary printable state	P50D1	Feasible but less favorable for dense multilayer printing
Low-structure rejected states	P50D2 and P52.5D2	Weak yield and low elastic recovery increase deformation risk
High-structure rejected state	P55D1	Excessive network strength increases clogging and drying sensitivity
Homogeneity-limited state	P55D2	Highest dispersant-to-other-liquid ratio and defect-prone behavior
Printable-height estimate	P52.5D1 from Eq. (3)	Approximately 3.42 mm
Extrusion condition	420 µm nozzle, 5 mm s^{-1}, 0.045 MPa	Stable deposition with controlled line width
Line-contact condition	Preferred $\Lambda_{ll} \approx 0.8$	Larger inter-filament contact and lower channel-void risk
Preferred firing condition	1200 °C, lead-rich atmosphere	High density without apparent phase degradation
Printed relative density	P52.5D1 route	97.59(46) %
Density difference from pressing	Eq. (5)	Approximately 0.14 percentage points
Functional response	Printed specimen after poling	$d_{33} \approx 268(10)$ pC/N

P52.5D1 is not a one-size-fits-all solution according to the findings in Table 3. Rather, this is the recipe needed to meet the needs of our particular matrix. If the powder grain size, binder content, nozzle length, drying conditions, or the sintering profile changes, the window can move accordingly. The important insight here is that the relationship between rheological properties, linearity, density, and d_{33} measurements is what is portable.

3. Results and Discussion

3.1. Composition and rheological window

The first result is that rheological properties of hard-PZT DIW ink have a bounded range, instead of showing a monotonic dependence either on the volume fraction of solids or the concentration of dispersants. Adding more solids (from 50 to 55 volume%) strengthens the structure and can increase the height of print. However, it increases the flow resistance which has to be overcome using a pneumatic delivery method. Doubling dispersant content (from 1 to 2 wt%) decreases the strength of structure at low concentrations of solids. However, the increased mobility does not improve the reliability of shape retaining. Thus, printable region is situated at the intermediate compositions.

Pastes P50D2 and P52.5D2 are situated on the left-hand end of the rheological window and show relatively low oscillatory yield stress (23.18 Pa and 49.05 Pa respectively). Maximum values of storage modulus are 6352 Pa and 8877 Pa. In both cases, these values are significantly lower than the rheological parameters of ink P52.5D1. Therefore, it is not possible to assume that increasing dispersant concentration automatically results in an improvement. Lowered viscosity can provide better conditions for shear deformation but insufficient recovery of the structure after that is undesirable in dense multilayer printing process [7,9,11,29].

P55D1 describes the other end of the window. The presence of its high oscillatory yield stress at 229.22 Pa and G'_{max} at 253 260 Pa suggests a high degree of self-supporting nature,

but at the same time, it increases the material's sensitivity to extrusion pressure. This effect is in agreement with previous studies on dense ceramics using DIW processes. In such cases, an extremely high solid loading increases the stiffness of the resulting green body, but also decreases the pressure window for successful deposition [10,12,13]. Therefore, P55D1 is also not chosen for further investigations for a completely different reason. Namely, unlike low-structure materials, it is too stiff rather than too fluid.

P52.5D1 demonstrates the best compromise as it maintains the required yield stress value and stiffness while staying in the processability range. With its oscillatory yield stress at 154.23 Pa and G'_{max} at 146 680 Pa, it is able to recover better compared to P50D1 but does not reach the stiffness of P55D1. At the same time, its printable height is predicted to be higher (3.42 mm vs 2.37 mm) and gives more tolerance to layer deformations. This explains why P52.5D1 was chosen for extrusion geometry tests.

Finally, the case of P55D2 highlights the importance of measuring the effectiveness of dispersant through homogeneity and recovery characteristics. P55D2 has the highest dispersant-to-the rest liquid ratio at 0.214 and demonstrates poor processing results as well [33]. This finding is consistent with previous suspension printing literature, where it was shown that the addition of the dispersant had an optimal range beyond which the dispersion stability or particle network integrity were decreased [23,28]. Therefore, the optimal ink should not be the least resistant, but have the controlled amount of resistance that allows for recovery.

3.2. Extrusion Matching and Filament Touches

When the rheological window has been set, there remains another constraint for P52.5D1: nozzle-scale manufacturability. The retained configuration will be using a 420 µm nozzle at 5 mm s^{-1} velocity, with an extrusion pressure close to 0.045 MPa. In other words, such values correspond to a matched operation. If the pressure was too low, there would have been under-delivery, whereas higher pressure values would have made the filament too broad. Higher velocity values would have increased the demand on the shear rate and would have created a line starvation, while lower velocities might have made it overfilled. The operating point thus makes sense since it ensures both continuity and precise shape.

Pressure matching is shown as a middle state for printing, as in Figure 4, rather than as a limiting condition. The under-delivered ring takes on an irregular shape, while the over-delivered ring takes a wider appearance, and the matched ring takes a continuously filled annular form. This photograph confirms the numerical operating point using a 420 µm nozzle at 5 mm s^{-1} travel speed and a pressure of about 0.045 MPa.

Λ_h plays a crucial role in the line-contact case. At small values of h/D, adjacent filaments are rounder and only in contact within a narrower cross-sectional distance. Thus, there will be gaps for the channel cavities to survive drying and sintering. Lowering the line height to 0.8 times the nozzle diameter will make the filament contact closer and thus reduce the chance of porosity between struts. Here, the influence of line geometry extends further than just aesthetic purposes. In the current PZT process, line geometry serves as the precursor to achieving a certain density since part of the porosity has already formed before firing.

The endpoint defect provides a second example of defect formation due to improper motion and not composition. If the nozzle stops or changes its direction suddenly, then the resulting residual pressure will lead to protrusions along the endpoint [33]. An outward movement of the blank will avoid the above defect since it allows the change in the pressure distribution and toolpath trajectory to be made separately. This shows that defect control in dense PZT DIW is not only a rheological problem. It also requires path design and pressure-release logic appropriate to the material response.

Close-up images in Figure 5 reveal the geometric portion of the answer. Contact is represented by filament stacks becoming one wall, whereas endpoint consists of locally excessive material due to the pressure left over from residual pressure at the end of the path. The relevance of this observation lies in the fact that both of the mentioned phenomena

could be present in the same ink material. P52.5D1 is only retained when the combination of material behavior and toolpaths controlling filament interaction and endpoint separation occurs.

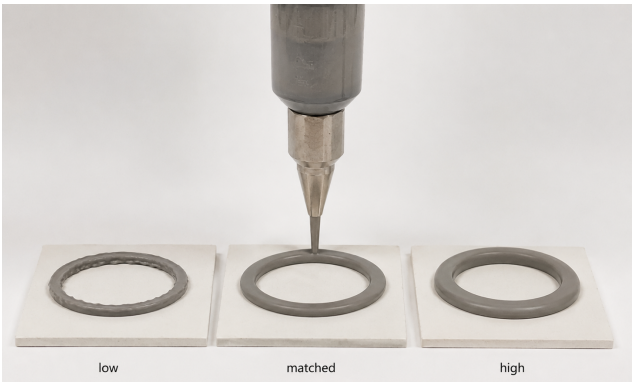

Figure 4. Pressure-matched ring deposition.

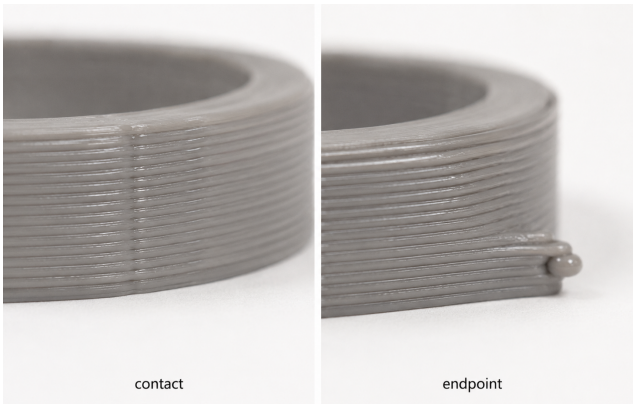

Figure 5. Filament contact and endpoint.

3.3. Densification, phase stability, and piezoelectric test

The last step in process verification is assessing whether the printed body becomes dense, phase-stable, and piezoelectric. The best obtained relative density value in retained DIW-printed specimens is 97.59(46) %, achieved at 1200 °C. The density of the die-pressed specimen was determined to be 97.73(39) %. The value obtained from Eq. (5) is about 0.14 percentage points. This number holds much importance, as it proves that the retained DIW condition does not incur a noticeable density penalty for printing rings of the desired geometry.

The comparison of fired rings in Figure 6 illustrates the relevance of the obtained density value. As seen, the DIW and die-pressed rings have identical appearance as fired ceramics, while the exposed cut surfaces serve as reminders of the evaluation criterion, which is density determined by bulk material consolidation. Compacting can increase the green body density, although not necessarily the fired density equally. Compacting affects the interconnection of porosity and gas pathways during burnout in the case of a printed body with organic substances and line-originated pores [33,39,40]. What really matters for optimization is obtaining the fired, phase-retained, and functional piece.

Phase and microstructural data lend credibility to the density results. There is no sign of a second phase or any phase shift detected in the XRD response following firing in the environment saturated with lead, suggesting effective lead loss control for the retained firing conditions [30,31]. Microscopy reveals the presence of a compact ceramic matrix without any visible delamination at interfaces of printed layers and having grains of approximately 1.2 µm. This is crucial since one cannot assume that the printed PZT body will be dense enough, while being prone to laminate defects or phase changes.

Figure 6. DIW and pressed fired rings.

The d_{33} result concludes the response to the research problem statement. As shown, the poling procedure yields $\pm 10\,\mathrm{pC/N}$ around $268\,\mathrm{pC/N}$. The value is consistent with the die-pressed specimen after poling, as well as the observed decline after 24 hours, corresponding to aging in typical ferroelectric ceramics [32,33,41,42]. While the exact values differ, the consistency of aging is what matters most: this proves that the directly written body maintains piezoelectric response similar to that produced by a conventionally processed sample.

The validation diagram in Figure 7 connects the final ceramic piece, the microstructure, and the piezoelectric measurement all in one picture. The ring shows that there is no macroscopic failure in the fired material, the microstructure inset provides a representative sample of the required dense grain structure for load transfer and poling, while the d_{33} meter gives a measure of the resulting functionality. All three provide consistency; hence, why P52.5D1 is termed as a functional DIW condition due to being dense in composition and not just printable paste.

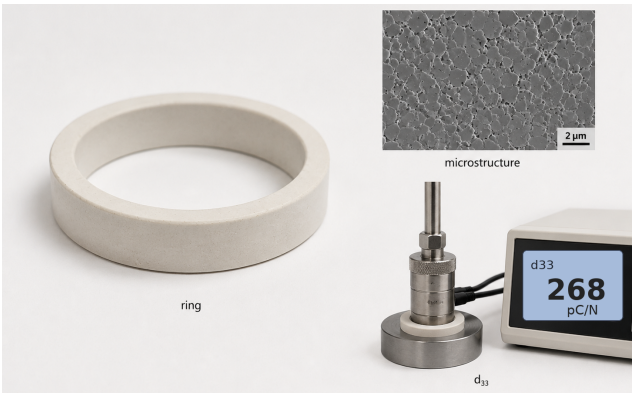

Figure 7. Ring microstructure and d_{33}.

3.4. Combined result of the six inks

These six ink compositions can now be understood as various failure or success scenarios. Ink P50D1 is printable, although P52.5D1 has better prospects due to having higher solids loading and higher estimate of printable height, which makes successful dense multilayer printing unlikely. Inks P50D2 and P52.5D2 both fail through weak recovery during extrusion. P55D1 fails due to overly strong structure and propensity to clog. P55D2 fails due to a combination of high dispersant/other liquid ratio, non-uniformity, and defect formation. P52.5D1 is the only ink that passed all criteria.

The outcome gallery of Figure 8 provides the most succinct answer possible to the research questions posed in this study. P52.5D1 is displayed here as the selected clean ring, whereas other samples highlight printed results characterized by poor inks recovery, rough surface creation, or disrupted annular structure. Thus, P52.5D1 is selected not on the basis of high solids concentration, low pressure application, or superior elastic modulus. Instead, it is selected because it excludes all principal failure modes: weak ink flows poorly, overly

structured inks clog or form a rough surface, suboptimal geometry creates void channels, rapid path termination creates local flaws, and compaction may not affect overall density.

Figure 8. Six-ink printing outcomes.

The lesson that can be generalized from the findings is the following: in future PZT-DIW studies, researchers need to provide sufficient information to identify a formulation based on a whole path of material properties, motion planning, and densification. A composition alone without information on rheology is incomplete; rheology information alone without data on line geometry is insufficient; line geometry alone without sintering density information is inadequate; and a density alone without the presence of phases and d_{33} values is incomplete. The six inks show that these variables are indeed not redundant. Each one detects a particular failure mode, while the decision about the manufacturing process is derived from reading all six at once.

4. Conclusion

In this paper, we investigated the question which material-state/operating condition combination in a matrix of six-ink hard-PZT direct writing conditions can simultaneously ensure the satisfaction of the following criteria: cohesive suspension, recoverable rheology, filaments' contact, tail defect prevention, densification, and piezoelectric response similar to the results obtained by die pressing. There was only one such combination among the investigated states – P52.5D1, consisting of 52.5 vol% PZT and 1 wt% dispersant, meeting all the requirements. This combination is not the heaviest ink, the ink with the lowest extrusion pressure, and the stiffest ink. This is an ink with a material structure compatible with the required movement and reaction of the nozzle.

Concerning rheological properties of ink, one should note that a useful ink should not have some extreme properties. P50D2 and P52.5D2 belong to the too weak pastes, because their oscillatory yield stresses are 23.18 Pa and 49.05 Pa, respectively, and their storage moduli are relatively low. Ink P55D1 has too strong structure, because its oscillatory yield stress is 229.22 Pa and $G'_{\max} = 253\,260$ Pa, which leads to clogging and pressure instability. Ink P52.5D1 is situated between two limits above and has sufficient strength, its oscillatory yield stress and storage modulus being equal to 154.23 Pa and 146 680 Pa, respectively. The height at which it can be printed is close to 3.42 mm.

Geometry and extrusion conditions also have their optimal parameters. Nozzle diameter 420 µm and velocity of 5 mm s^{-1} and about 0.045 MPa provide stable delivery and control of the filament width. Optimal h/D value of about 0.8 ensures good contact between the filaments and reduces the likelihood of channel voids. Moreover, blank moving outward at the tail prevents tail defects.From the previous analysis, it can be seen that the

retained printing route is an example of a material-motion state rather than just material composition.

The densification and functional parts of the answers indicate that the retained printed sample attains its final dense ceramic structure comparable to die pressed specimens. At 1200 °C with a Pb rich atmosphere, the density of the printed specimens is about 97.59(46) %, and for the die pressed specimens, it is about 97.73(39) %. In other words, the difference in densities is very small (about 0.14 percentage points). Finally, the retention of phases, dense microstructure, lack of noticeable interlayer delamination, and $d_{33} \approx 268(10)$ pC/N confirms that the printed sample maintains its functional properties.

In summary, dense functional direct ink-writing of PZT is achieved through compatibility of all processes involved. The composition of ink, rheological recovery, matching of speed-pressure, filament contacts, endpoint motion, ceramic forming process, and the d_{33} measurements have revealed their own respective failures and hence should all be taken into account when assessing the feasibility of dense direct written hard-PZT ceramics. In the explored six-ink sample space, P52.5D1 yields the strongest results towards this aim.

References

[1] Lakhdar, Y., Tuck, C., Binner, J., Terry, A., & Goodridge, R. (2021). Additive manufacturing of advanced ceramic materials. Progress in Materials Science, 116, 100736.

[2] Chen, Z., Li, Z., Li, J., Liu, C., Lao, C., Fu, Y., ... & He, Y. (2019). 3D printing of ceramics: A review. Journal of the European Ceramic Society, 39(4), 661-687.

[3] Cramer, C. L., Ionescu, E., Graczyk-Zajac, M., Nelson, A. T., Katoh, Y., Haslam, J. J., ... & Minary-Jolandan, M. (2022). Additive manufacturing of ceramic materials for energy applications: Road map and opportunities. Journal of the European Ceramic Society, 42(7), 3049-3088.

[4] Chen, Z., Sun, X., Shang, Y., Xiong, K., Xu, Z., Guo, R., ... & Zheng, C. (2021). Dense ceramics with complex shape fabricated by 3D printing: A review. Journal of Advanced Ceramics, 10(2), 195-218.

[5] Rocha, V. G., Saiz, E., Tirichenko, I. S., & García-Tuñón, E. (2020). Direct ink writing advances in multi-material structures for a sustainable future. Journal of Materials Chemistry A, 8(31), 15646-15657.

[6] Smay, J. E., Gratson, G. M., Shepherd, R. F., Cesarano III, J., & Lewis, J. A. (2002). Directed colloidal assembly of 3D periodic structures. Advanced Materials, 14(18), 1279-1283.

[7] Smay, J. E., Cesarano, J., & Lewis, J. A. (2002). Colloidal inks for directed assembly of 3-D periodic structures. Langmuir, 18(14), 5429-5437.

[8] Lewis, J. A., Smay, J. E., Stuecker, J., & Cesarano, J. (2006). Direct ink writing of three-dimensional ceramic structures. Journal of the American Ceramic Society, 89(12), 3599-3609.

[9] Lewis, J. A. (2006). Direct ink writing of 3D functional materials. Advanced Functional Materials, 16(17), 2193-2204.

[10] Rueschhoff, L., Costakis, W., Michie, M., Youngblood, J., & Trice, R. (2016). Additive manufacturing of dense ceramic parts via direct ink writing of aqueous alumina suspensions. International Journal of Applied Ceramic Technology, 13(5), 821-830.

[11] M'barki, A., Bocquet, L., & Stevenson, A. (2017). Linking rheology and printability for dense and strong ceramics by direct ink writing. Scientific reports, 7(1), 6017.

[12] Lakhdar, Y., Tuck, C., Terry, A., Spadaccini, C., & Goodridge, R. (2021). Direct ink writing of boron carbide monoliths. Journal of the European Ceramic Society, 41(16), 76-92.

[13] Kemp, J. W., Diaz, A. A., Malek, E. C., Croom, B. P., Apostolov, Z. D., Kalidindi, S. R., ... & Rueschhoff, L. M. (2021). Direct ink writing of ZrB2-SiC chopped fiber ceramic composites. Additive Manufacturing, 44, 102049.

[14] Jaffe, H. (1958). Piezoelectric ceramics. Journal of the American Ceramic Society, 41(11), 494-498.

[15] Haertling, G. H. (1999). Ferroelectric ceramics: history and technology. Journal of the American Ceramic Society, 82(4), 797-818.

[16] Narita, F., & Fox, M. (2018). A review on piezoelectric, magnetostrictive, and magnetoelectric materials and device technologies for energy harvesting applications. Advanced Engineering Materials, 20(5), 1700743.

[17] Hao, J., Li, W., Zhai, J., & Chen, H. (2019). Progress in high-strain perovskite piezoelectric ceramics. Materials Science and Engineering: R: Reports, 135, 1-57.

[18] Kalem, V., Çam, İ., & Timuçin, M. (2011). Dielectric and piezoelectric properties of PZT ceramics doped with strontium and lanthanum. Ceramics International, 37(4), 1265-1275.

[19] Mahajan, S., Thakur, O. P., & Prakash, C. (2007). Effect of Sintering Temperature on Structural and PiezoelectricProperties of PNN-PZT Ceramics. Defence Science Journal, 57(1), 23-28.

[20] Maiwa, H., Kimura, O., Shoji, K., & Ochiai, H. (2005). Low temperature sintering of PZT ceramics without additives via an ordinary ceramic route. Journal of the European Ceramic Society, 25(12), 2383-2385.

[21] Liu, W., Xu, J., Lv, R., Wang, Y., Xu, H., & Yang, J. (2014). Effects of sintering behavior on piezoelectric properties of porous PZT ceramics. Ceramics International, 40(1), 2005-2010.

[22] Liu, K., Zhang, Q., Zhou, C., Shi, Y., Sun, C., Sun, H., ... & Fu, Y. (2021). 4D printing of lead zirconate titanate piezoelectric composites transducer based on direct ink writing. Frontiers in Materials, 8, 659441.

[23] Walton, R. L., Fanton, M. A., Meyer Jr, R. J., & Messing, G. L. (2020). Dispersion and rheology for direct writing lead-based piezoelectric ceramic pastes with anisotropic template particles. Journal of the American Ceramic Society, 103(11), 6157-6168.

[24] Hall, S. E., Regis, J. E., Renteria, A., Chavez, L. A., Delfin, L., Vargas, S., ... & Lin, Y. (2021). Paste extrusion 3D printing and characterization of lead zirconate titanate piezoelectric ceramics. Ceramics International, 47(15), 22042-22048.

[25] Nan, B., Olhero, S., Pinho, R., Vilarinho, P. M., Button, T. W., & Ferreira, J. M. (2019). Direct ink writing of macroporous lead-free piezoelectric Ba0. 85Ca0. 15Zr0. 1Ti0. 9O3. Journal of the American Ceramic Society, 102(6), 3191-3203.

[26] NAN, B., ZANG, J., LU, W., YANG, T., ZHANG, S., & ZHANG, H. (2022). Recent progress on additive manufacturing of piezoelectric ceramics. Journal of Inorganic Materials, 37(6), 585-595.

[27] Wätjen, A. M., Gingter, P., Kramer, M., & Telle, R. (2014). Novel prospects and possibilities in additive manufacturing of ceramics by means of direct inkjet printing. Advances in Mechanical Engineering, 6, 141346.

[28] Muniz, N. O., Vechietti, F. A., & Santos, L. A. (2015). Effect of variation of dispersant and fluid in the rapid prototyping of alumina. Key Engineering Materials, 631, 275-279.

[29] del-Mazo-Barbara, L., & Ginebra, M. P. (2021). Rheological characterisation of ceramic inks for 3D direct ink writing: A review. Journal of the European Ceramic Society, 41(16), 18-33.

[30] Safar, M., Button, T. W., & Zabcik, M. (2017, May). Control of PbO loss during sintering of PZT: Laboratory vs industry. In 2017 Joint IEEE International Symposium on the Applications of Ferroelectric (ISAF)/International Workshop on Acoustic Transduction Materials and Devices (IWATMD)/Piezoresponse Force Microscopy (PFM) (pp. 83-88). IEEE.

[31] Hao, X., Zhai, J., Kong, L. B., & Xu, Z. (2014). A comprehensive review on the progress of lead zirconate-based antiferroelectric materials. Progress in materials science, 63, 1-57.

[32] Genenko, Y. A., Glaum, J., Hoffmann, M. J., & Albe, K. (2015). Mechanisms of aging and fatigue in ferroelectrics. Materials Science and Engineering: B, 192, 52-82.

[33] Hossain, S. S., Jang, S., Park, S., & Bae, C. J. (2023). Understanding ink design and printing dynamics of extrusion-based 3D printing: Defect-free dense piezoelectric ceramics. Journal of Manufacturing Processes, 92, 1-11.

[34] Hershell, W. H., & Bulkey, R. (1926). Konsistenzmessungen von Gummi-Benzollosungen. Kolloid Zeitschrift, 39, 291.

[35] Chen, T., Sun, A., Chu, C., Wu, H., Wang, J., Wang, J., ... & Xu, G. (2019). Rheological behavior of titania ink and mechanical properties of titania ceramic structures by 3D direct ink writing using high solid loading titania ceramic ink. Journal of Alloys and Compounds, 783, 321-328.

[36] An, T., Hwang, K. T., Kim, J. H., & Kim, J. (2020). Extrusion-based 3D direct ink writing of NiZn-ferrite structures with viscoelastic ceramic suspension. Ceramics International, 46(5), 6469-6476.

[37] Pospischil, M., Specht, J., König, M., Hörteis, M., Mohr, C., Clement, F., & Biro, D. (2013). Paste rheology correlating with dispensed finger geometry. IEEE Journal of Photovoltaics, 4(1), 498-503.

[38] Sweeney, M., Campbell, L. L., Hanson, J., Pantoya, M. L., & Christopher, G. F. (2017). Characterizing the feasibility of processing wet granular materials to improve rheology for 3D printing. Journal of Materials Science, 52(22), 13040-13053.

[39] Papitha, R., Suresh, M. B., Rao, Y. S., Saha, B. P., Das, D., & Johnson, R. (2013). Pressure slip casting and cold isostatic pressing of aluminum titanate green ceramics: A comparative evaluation. Processing and Application of Ceramics, 7(4), 159-166.

[40] Popov, V., Fleisher, A., Muller-Kamskii, G., Avraham, S., Shishkin, A., Katz-Demyanetz, A., ... & Goel, S. (2021). Novel hybrid method to additively manufacture denser graphite structures using Binder Jetting. Scientific Reports, 11(1), 2438.

[41] Kumar, A., Bhanu Prasad, V. V., James Raju, K. C., & James, A. R. (2015). Optimization of poling parameters of mechanically processed PLZT 8/60/40 ceramics based on dielectric and piezoelectric studies. The European Physical Journal B, 88(11), 287.

[42] Li, Y. W., Zhou, X. L., Miao, H. C., Cai, H. R., & Li, F. X. (2013). Mechanism of crystal-symmetry dependent deformation in ferroelectric ceramics: Experiments versus model. Journal of Applied Physics, 113(21).